Chinese Chemical Letters 37 (2026) 112476

Contents lists available at ScienceDirect

Chinese Chemical Letters

journal homepage: www.elsevier.com/locate/cclet

Mechanisms of membrane fouling alleviation by Fe(II)/Fe(VI)-activated sodium sulfite pretreatment in membrane distillation

Yuan Huang[a,b,1], Suhua Gu[a,b,1], Haiqing Chang[a,b,*], Bo Lai[b]

[a] State Key Laboratory of Intelligent Construction and Healthy Operation and Maintenance of Deep Underground Engineering, Sichuan University, Chengdu 610065, China
[b] College of Architecture and Environment, Sichuan University, Chengdu 610207, China

ARTICLE INFO

Article history:
Received 16 October 2025
Revised 26 January 2026
Accepted 28 January 2026
Available online 17 July 2026

Keywords:
Membrane distillation (MD)
Shale gas produced water (SGPW)
Sodium sulfite
Membrane fouling
Thermal activation

ABSTRACT

Membrane distillation (MD) suffers from severe fouling when treating high-salinity and high-organic shale gas produced water (SGPW). This study introduces a Fe(II)/Fe(VI)-activated sodium sulfite (Na_2SO_3) pretreatment that generates sulfate radicals with high pH tolerance and strong organic degradation capacity. The process achieved total organic carbon (TOC) removals of 17.82 % (Fe(II)) and 13.83 % (Fe(VI)) and maintained MD flux at 80.95 %-85.70 % of the initial value, while permeate conductivity decreased by 23.46 % and 28.74 %. Pollutant deposition decreased by 44.32 % and 61.79 %, with liquid entry pressure recovering to 89.20 % and 90.86 % of original value. Scanning electron microscope and Fourier transform infrared spectroscopy confirmed significant fouling layer reduction and maintained membrane hydrophobicity. Mechanistic studies indicate pretreatment optimizes fouling behavior by regulating organic concentration, hydrophilic/hydrophobic distribution, and coagulation efficiency. This work provides an efficient, low-cost green pretreatment for SGPW and deepens understanding of multi-mechanism fouling control by Na_2SO_3 oxidation.

© 2026 Published by Elsevier B.V. on behalf of Chinese Chemical Society and Institute of Materia Medica, Chinese Academy of Medical Sciences.

With the global push toward carbon neutrality, energy structure transformation has become a strategic imperative for sustainable development [1–3]. As a transitional energy source, shale gas-characterized by abundant reserves and low carbon emissions-is reshaping the global energy landscape through continuous technological and industrial advancements [4–7]. Hydraulic fracturing in shale gas extraction involves injecting large volumes of freshwater, chemical additives and proppants into the formation using high-pressure pumps [5,8,9]. Typically, each well requires between 6700 m^3 and 60,000 m^3 of water, of which approximately 5 %–85 % returns to the surface as flowback and produced water-collectively referred to as shale gas produced water (SGPW) [10,11]. SGPW is characterized by high organic matter and high salinity, posing a huge challenge to treatment processes [8,9,12,13]. Membrane distillation (MD), as a new type of heat-driven membrane separation technology, has become an ideal method for treating high-salt organic wastewater due to its ability to achieve a retention rate of nearly 99 % for soluble substances and its good compatibility with industrial waste heat or solar heat sources [12,14].

Although MD offers numerous advantages in treating high-salinity wastewater, membrane fouling can lead to reduced operational efficiency and shortened membrane lifespan [15–19]. The essence of membrane fouling is the physical deposition or chemical adsorption of pollutants on the membrane surface or within the membrane pores [9,14]. Pollutant deposition can cause irreversible decreases in membrane flux, increased mass transfer resistance, and pore wetting, leading to deterioration of membrane retention performance and reduced membrane separation efficiency [14,20]. Therefore, addressing membrane fouling issues is critical to the widespread application of membrane distillation technology. Based on the source of contaminants and their mechanisms of action, membrane fouling primarily manifests in three typical forms: inorganic fouling, organic fouling, and biological fouling [21–24]. Among these, organic fouling-a common factor affecting MD performance-is caused by the adsorption and accumulation of organic matter on the membrane surface [25]. Therefore, in controlling membrane fouling caused by SGPW, it is essential to focus on analyzing these organic fouling to mitigate the resulting membrane fouling.

To address the challenge of membrane fouling, current research primarily focuses on three areas: Operating conditions, membrane modification and pretreatment [26–29]. Pre-treatment, owing to its low cost and high efficiency, is frequently employed as a

* Corresponding author.
E-mail address: changingchq@126.com (H. Chang).
[1] These authors contributed equally to this work.

https://doi.org/10.1016/j.cclet.2026.112476
1001-8417/© 2026 Published by Elsevier B.V. on behalf of Chinese Chemical Society and Institute of Materia Medica, Chinese Academy of Medical Sciences.

method to mitigate membrane fouling in MD for wastewater treatment [17,30–32]. Various pre-treatment strategies have been developed to mitigate membrane fouling in MD, primarily including coagulation, adsorption, filtration, advanced oxidation and membrane technology [28,33–35]. These techniques have been proven to effectively mitigate membrane fouling and maintain MD performance. Existing research has clearly indicated that the concentration of organic matter in SGPW is a key factor influencing membrane fouling [9].

Sodium sulfite (Na_2SO_3) is a common industrial by-product with low cost, abundant availability and excellent environmental compatibility [36–39]. Its aqueous residues can be readily converted into non-toxic sulfates through aeration. Compared with commonly used oxidants such as peroxydisulfate and percarbonate, sodium sulfite possesses higher selectivity toward hydrophobic organics, lower activation energy and better adaptability across a wide pH range [36,40]. In advanced oxidation processes, sulphite radicals ($SO_4^{\bullet-}$) have attracted attention due to their ability to degrade various pollutants [41,42]. Related studies indicate that under the activation of Fe(VI) and Fe(II), sodium sulfite can be efficiently converted into $SO_4^{\bullet-}$, not only effectively degrading organic matter but also alleviating nanofiltration membrane fouling [41]. Cao *et al*. used nitrogen-doped graphite nitride carbon photocatalytic activation of sulfite to generate sulfate radicals for the efficient degradation of carbamazepine. It is evident that the sodium sulfite oxidation system is a promising pretreatment strategy with potential application value in mitigating membrane fouling in MD [43].

In this study, we developed an efficient Fe(VI)/Na_2SO_3 pre-oxidation system to mitigate membrane fouling during the SGPW membrane-based hierarchical treatment process by optimizing the catalyst-to-oxidant ratio. This system leverages the dual oxidation-flocculation functionality of Fe(VI) and the radical-generating capability of Na_2SO_3 to enhance pre-treatment performance while minimizing chemical consumption. We systematically investigated the following aspects: (1) The pollutant removal efficiency of Fe(VI)/Na_2SO_3 in SGPW treatment, (2) its impact on MD system performance, (3) membrane fouling mitigation effects and (4) the relationship between water quality and fouling behavior, including an in-depth analysis of the fouling mitigation mechanisms.

The SGPW was sourced from the shale gas extraction area in Luxian County, Sichuan Basin, with its characteristics listed in Table S1 (Supporting information). Turbidity was measured by TL2310 turbidity meter (Hach Company, USA). Ultraviolet absorbance (UV_{254}) was measured by UV-100 ultraviolet-visible spectrophotometer (Shanghai Mapada Instrument Co., Ltd., China). Total organic carbon (TOC) was determined by Liquid TOC II analyzer (Analytik Jena AG, Germany). Hydrophilic and hydrophobic organic compounds were separated using resins. XAD-8 resin (Shanghai Yika Biotechnology Co., Ltd., China) was used to adsorb hydrophobic organic compounds, XAD-4 resin (Shanghai McLean Bio-Chemical Technology Co., Ltd., China) was used to adsorb transitional organic compounds, while hydrophilic organic compounds in the system passed through both resins. The excitation-emission matrix (EEM, Hitachi, Ltd., Japan) is determined using a fluorescence spectrometer. The EEM spectra were analyzed using fluorescence region integration (FRI) technology (Section S2 in Support information). The reactive oxygen species (ROS) was characterized by electron paramagnetic resonance (ESR/EPR, Germany Magnettech ESR MS 5000X, Germany) [44]. The oxidation system was reduced to 5 mL and the capture of $SO_4^{\bullet-}$ was carried out by adding 20 μL 5,5-dimethyl-1-pyrroline *N*-oxide (DMPO, analytical purity, Shanghai Macklin Biochemical Co., Ltd., China) using ESR. High-priced iron (IV/V) characterized using methyl phenyl sulfonyl (PMSO, analytical purity, Shanghai Macklin Biochemical Co., Ltd., China) [44], and the oxidation product of PMSO by high-priced iron(IV/V) is $PMSO_2$ (methyl phenyl sulfone, Shanghai Macklin Biochemical Co., Ltd., China), the calibration curves of PMSO and $PMSO_2$ are in Figs. S1 and S2 (Support information).

Commercial polyvinylidene fluoride (PVDF) membranes (0.45 μm, IPVH00010, Millipore, Ireland) used for laboratory-scale DCMD exhibit high hydrophobicity, with a water contact angle (WCA) of 126.00°. Qualitative filter paper (diameter 18 cm, model 101, Fushun Civil Affairs Filter Paper Co., Ltd., China) was used for filtration. Deionized water was used to prepare solutions, produced by an ultra-pure water purification system (UPT-II-10T, Ulupure, Chengdu, China). Heptahydrate ferrous sulfate (Fe(II)) and sodium sulfite (Na_2SO_3) were sourced from Chengdu Kolon Chemical Co., Ltd. Potassium ferrate (K_2FeO_4) was purchased from Hubei Chushengwei Chemical Co., Ltd.

The functional groups of contaminants on the membrane surface were measured using an attenuated total reflection Fourier transform infrared (FTIR) spectrometer (model IRAffinity-1S, Shimadzu Corporation, Japan). 2D FTIR spectra were obtained by applying Yang's method [45], where synchronous maps reveal correlated intensity changes at different wavenumbers, and asynchronous maps highlight sequential or independent spectral variations. The liquid entry pressure (LEP) was determined using a homemade device combined with ultra-pure water (Section S4 in Support information). The mechanical strength of the membrane was analyzed using a tensile tester (AG-X, 10 kN, Shimadzu Corporation, Japan). The elemental composition and morphology of contaminants deposited on the membrane surface were analyzed using an XMAXN energy dispersive spectrometer (EDS, Oxford Instruments, UK) and scanning electron microscope (SEM, REGULUS-8230, Hitachi, Japan). Prior to testing, membrane samples were gold-plated under an accelerated voltage of 5 kV. The contact angles of new membranes and membranes after MD were measured using a JC2000D4 contact angle measuring instrument (POWEREACH, Shanghai Zhongchen Company, China). FTIR spectra were scanned 20 times at a resolution of 4 cm^{-1} in the wavenumber range of 400–4000 cm^{-1}. Surface tension was calculated based on the Extended Derjaguin-Landau-Verwey-Overbeek (XDLVO) theory (Section S5 in Supporting information). Partial least squares path modeling (PLS-PM) was used to establish the relationship between EEM, hydrophobic organic fraction (HPO) & hydrophilic organic fraction (HPI), surface tension, and membrane fouling. This modeling process was completed using RStudio (version 2023.12.1 + 402) equipped with the plspm package.

The experimental setup is shown in Fig. S4 (Supporting information), employing different oxidation strategies for pretreatment, including three activation methods: Fe(II), Fe(VI) and thermal energy: (a) Na_2SO_3 single-factor experiment: Investigating the treatment efficiency at concentration gradients of 0.5–3 mmol/L under normal/high temperatures (25/50 °C), (b) Fe(II)/Na_2SO_3 system: With sodium sulfite fixed at 1 mmol/L, the inhibitory effect on membrane fouling was studied at molar ratios of 0.5–1.5 under normal/high temperatures (25/50 °C) and (c) Fe(VI)/Na_2SO_3 system: Under the same conditions as (b), the synergistic effect of high-valent iron was investigated.

Fig. 1 shows the water quality variations of SGPW treated with sodium sulfite under different activation conditions. Sodium sulfite alone exhibited negligible purification, achieving only 4.90 %, 1.80 % and 1.77 % removal of UV_{254}, TOC and ammonia nitrogen at ambient temperature, with the HPO decreasing slightly from 52.19 % to 49.12 % (Figs. 1a-d). Heating to 50 °C modestly improved UV_{254} and TOC removal to 5.40 % and 4.52 %, indicating that temperature enhances its oxidative action. In contrast, iron-based activation substantially improved treatment performance. At room temperature, the Fe(II)-activated system achieved 13.33 %, 12.64 % and 22.68 % removal of UV_{254}, TOC and ammonia nitrogen, while Fe(VI)-activation yielded 10.00 %, 10.32 % and 26.60 %, with the

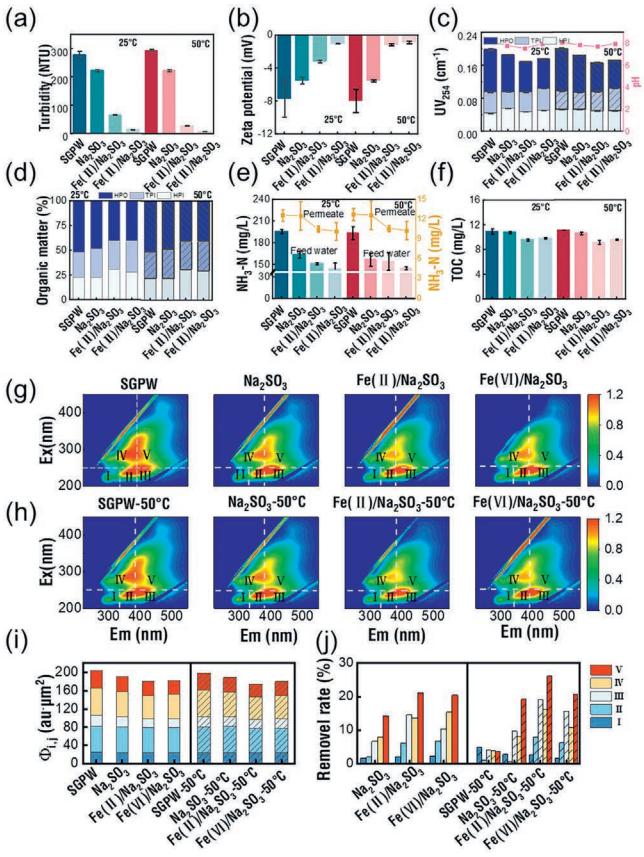


Fig. 1. Effect of Na_2SO_3, Fe(II)/Na_2SO_3 and Fe(VI)/Na_2SO_3 treatment on water quality: (a) UV_{254}, (b) UV_{254} fractions (*i.e.*, HPO/TPI/HPI ratio), (c) ammonia nitrogen concentrations, (d) TOC, (e) turbidity, (f) zeta potential, (g) EEM fluorescence spectra of influent (25 °C), (h) EEM fluorescence spectra of influent (50 °C), (i) the normalized EEM area volumes ($\Phi_{i,n}$) and (j) the removal rate in the normalized EEM area of SGPW. Note: Region I (aromatic compounds), Region II (aromatic proteins), Region III (furic acid), Region IV (soluble microbial product-like substances) and Region V (humic acid). Condition: Fe(II) = 1 mmol/L, Fe(VI) = 1 mmol/L, Na_2SO_3 = 2 mmol/L, SGPW = 200 mL.

HPO fraction dropping to 40.72 % and 40.89 %, respectively. Thermal activation further enhanced removal, reaching 17.82 % TOC and 21.16 % ammonia nitrogen for Fe(II)-activation and 13.83 % and 25.89 % for Fe(VI)-activation, with HPO declining to 40 %. These results demonstrate that thermal activation promotes radical generation and thus improves organic degradation efficiency [46,47]. Among the systems tested, Fe(II)-activation yielded superior performance, particularly for hydrophobic organics [48]. Mechanistically, Fe(II) activation promotes sulfate radical generation, driving effective oxidation and decomposition of organic compounds. Additionally, *in-situ* formed Fe(III) contributes to coagulation and adsorption, further facilitating contaminant removal [49,50]. Mechanistically, Fe(II)-activation generates sulfate radicals to oxidize organics while *in-situ* Fe(III) facilitates coagulation and adsorption, whereas Fe(VI)-activation produces high-valent Fe species (Fe(V), Fe(IV)) and reactive radicals ($^{\bullet}OH$, $SO_4^{\bullet-}$) with similar synergistic effects. The slightly lower performance of Fe(VI) likely stems from its pH-dependent hydrolysis being inhibited at the alkaline pH (8.04) induced by sodium sulfite [51]. Overall, Fe(II)-activated sodium sulfite exhibited superior removal of hydrophobic organic matter compared to Fe(VI)-activation.

To elucidate the degradation behavior of fluorescent organic matter in SGPW, EEM spectroscopy coupled with FRI was conducted (Figs. 1g and h) [52]. Sodium sulfite alone showed limited removal, reducing total fluorescence by 6.54 % at room temperature and 7.70 % at 50 °C, indicating modest temperature-enhanced oxidation. In contrast, iron-based activation markedly improved removal. At room temperature, total fluorescence decreased by 11.64 % and 10.86 % under Fe(II)- and Fe(VI)-activation, respectively, increasing to 14.48 % and 11.76 % at 50 °C. Notably, humic-like substances (Region V), a major fraction of recalcitrant dissolved organic matter, were substantially removed-21.16 % (Fe(II)) and 20.47 % (Fe(VI)) at room temperature, rising to 26.13 % and 20.83 % at 50 °C. These results demonstrate that Fe(II)-activated sodium sulfite exhibits superior degradation of fluorescent and humic-like organics, with thermal activation further enhancing treatment efficiency.

Different pretreatment systems also regulated the colloidal stability of SGPW (Figs. 1e and f). The raw water exhibited a turbidity of 278 NTU and a zeta potential of −7.72 mV, indicating a high concentration of suspended solids with negatively charged surfaces. This suggests a mildly unstable colloidal system, which is consistent with previously reported findings [48,53]. Sodium sulfite alone slightly improved stability at room temperature, increasing the zeta potential to −5.54 mV and reducing turbidity by 19.96 %, but heating to 50 °C reversed this effect (−7.95 mV, 3.02 % turbidity), suggesting thermal destabilization of colloids. In contrast, iron-based activation markedly enhanced coagulation. At room temperature, Fe(II)- and Fe(VI)-activated systems raised the zeta potential to −3.20 and −1.04 mV and reduced turbidity by 76.29 % and 94.99 %, respectively. Under thermal activation, these effects intensified (−1.19 and −0.87 mV; 90.05 % and 97.27 % turbidity removal). This improvement is attributed to the *in-situ* formation of positively charged Fe(III) species with strong coagulant properties [54]. Fe(VI)-activation exhibited the strongest effect, further enhanced by heating, likely due to the dual role of Fe(VI) as both oxidant and coagulant, with its hydrolysis generating nanoscale Fe(III) that promotes coagulation and adsorption.

Collectively, these findings indicate that the introduction of iron-based activators significantly enhances the degradative capacity of sodium sulfite toward fluorescent organic matter. Among the two activators, Fe(II) consistently demonstrated superior performance compared to Fe(VI). In addition, thermal activation played a crucial role in amplifying the overall oxidation efficiency. The sodium sulfite oxidation systems, particularly under Fe(II) activation, also exhibited strong capabilities for targeting humic-like substances.

Fig. 2 and Fig. S5 (Supporting information) systematically compare the MD performance of raw and pretreated SGPW, highlighting the influence of various pretreatment conditions on membrane fouling mitigation. The results showed that untreated feedwater led to a dramatic decline in final normalized flux to 0.42 and a high permeate conductivity of 59.29 μS/cm, indicating severe deterioration of membrane performance. This observation aligns well with established membrane fouling theories, wherein organic and inorganic contaminants accumulate on the membrane surface, leading to flux loss and degraded separation efficiency [18,48]. Pretreatment with sodium sulfite improved MD performance to varying extents. Specifically, at room temperature, standalone sodium sulfite pretreatment increased the final normalized flux by 38.10 % and reduced conductivity by 18.76 %. Upon thermal activation at 50 °C, these improvements further increased to 47.62 % (flux) and 22.36 % (conductivity), consistent with the water quality enhancements reported in Fig. 1.

The introduction of iron-based activators resulted in substantial enhancements. Under ambient conditions, Fe(II)- and Fe(VI)-activated sodium sulfite systems increased the final normalized flux to 69.05 % and 80.95 %, respectively, while reducing permeate conductivity by 24.93 % and 28.74 %. Under thermal activation (50 °C), the flux rose further to 80.95 % and 85.70 %, with corresponding conductivity reductions of 23.46 % and 28.05 %. These re-

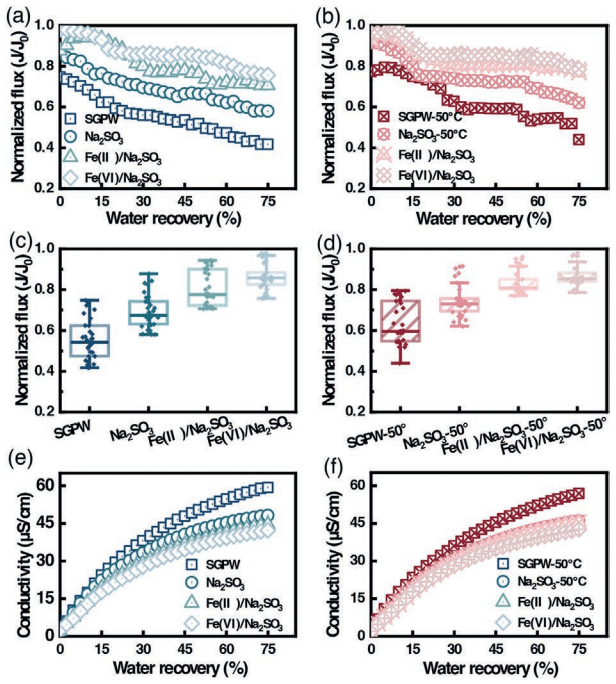


Fig. 2. Effect of Na_2SO_3, Fe(II)/Na_2SO_3 and Fe(VI)/Na_2SO_3 treatment on MD Performance: (a-d) Normalized MD flux and (e, f) conductivity with or without pretreatment under room temperature (25 °C) and heated (50 °C) conditions. Condition: Fe(II) = 1 mmol/L, Fe(VI) = 1 mmol/L, Na_2SO_3 = 2 mmol/L, SGPW = 200 mL.

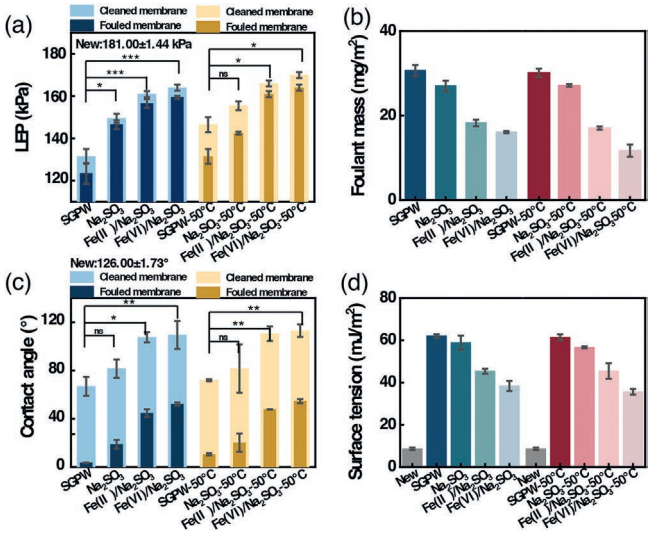


Fig. 3. Effect of Na_2SO_3, Fe(II)/Na_2SO_3 and Fe(VI)/Na_2SO_3 pretreatment on membrane surface properties: (a) LEP, (b) mass of deposited foulants, (c) Water contact angle (WCA) and (d) surface tension on the membrane surface of SGW under room temperature (25 °C) and heated (50 °C) conditions. Note: * $P < 0.05$, ** $P < 0.01$, *** $P < 0.001$. Condition: Fe(II) = 1 mmol/L, Fe(VI) = 1 mmol/L, Na_2SO_3 = 2 mmol/L, SGPW = 200 mL.

sults strongly indicate a synergistic effect between thermal and iron-based activation, which significantly alleviates membrane flux decline even at low reagent concentrations. Correlation analysis between membrane performance and water quality parameters further elucidated the underlying mechanisms. It is worth noting that the Fe(VI) activation system performs exceptionally well in terms of improving flux. This can be attributed to the dual functionality of Fe(VI), which not only generates strong oxidizing species and activates sodium sulfite, but also hydrolyzes to form Fe(III), an effective coagulant. This dual-action mechanism enhances the removal of organic matter through both oxidation and coagulation pathways.

Figs. 3a and b show the changes in LEP and foulant mass between pristine and fouled membranes. Using untreated SGPW as feedwater reduced the LEP from 181 kPa to 123.5 kPa and deposited 30.65 mg/m^2 of foulants, confirming the coupled effects of fouling and surface wetting, as described in previous research [14]. Sodium sulfite pretreatment partially mitigated these effects: At room temperature, it achieved 81.16 % LEP recovery and an 11.88 % reduction in foulants, while thermal activation yielded similar pollutant removal (11.48 %) but slightly lower LEP recovery (78.95 %). In contrast, iron-based activation provided greater improvements. The Fe(II)-activated system achieved 86.70 % LEP recovery and a 40.42 % reduction in foulants at room temperature, increasing to 89.20 % and 44.32 % under thermal activation. The Fe(VI)-activated system showed the best performance, with 88.37 % LEP recovery and 47.57 % foulant reduction at room temperature, further improving to 90.86 % and 61.79 % at 50 °C. These results demonstrate the superior antifouling efficacy of Fe(VI)-activation, attributed to its dual role in generating reactive oxidants and forming Fe(III) coagulants that synergistically remove dissolved and particulate foulants.

As shown in Figs. 3c and d and Table S2 (Supporting information), the pristine PVDF membrane exhibited strong hydrophobicity (contact angle: 126.00° ± 1.73°, surface energy: 8.63 mJ/m^2). After MD with raw SGPW, the contact angle dropped to 3.60° ± 0.27° (−97.14 %) and surface energy rose to 61.69 mJ/m^2, indicating formation of a hydrophilic fouling layer that severely impaired surface properties. Physical cleaning recovered only 53.10 % of the original contact angle, suggesting irreversible damage. Sodium sulfite alone provided limited restoration: At room temperature, contact angle recovered to 16.07 % and surface energy decreased to 56.65 mJ/m^2, while thermal activation yielded similar results (15.00 %). In contrast, iron-activated systems showed markedly better recovery. At room temperature, Fe(II)- and Fe(VI)-activation restored 35.48 % and 41.44 % of the contact angle (surface energy 45.40 and 38.40 mJ/m^2), increasing after cleaning to 85.38 % and 86.94 %. Under thermal activation, contact angle further rose to 37.93 % and 43.35 % with lower surface energies (45.45 and 35.61 mJ/m^2), and post-cleaning recovery reached 87.71 % and 89.71 %, respectively.

Figs. 4a-d present the scanning electron microscopy-energy dispersive spectrometer (SEM-EDS) evidence of membrane fouling formation and mitigation [55]. After MD with raw SGPW, a dense fouling layer fully covered the membrane surface (Figs. 4a and b); the characteristic fluorine (F) signal disappeared, oxygen (O) content increased from 0 % to 30.32 %, and new Si and Fe signals emerged (Figs. 4c and d), indicating deposition of an oxygen-rich fouling layer [56]. Sodium sulfite alone slightly alleviated fouling, reducing O content to 29.54 % and loosening the fouling structure. Iron-based activation achieved markedly stronger effects. At room temperature, the Fe(II)-activated system restored F to 32.21 % and reduced O to 7.48 %, further improving to 35.52 % F and 3.88 % O under thermal activation. Fe(VI)-activation performed best, increasing F to 41.35 % and reducing O to 5.78 % at room temperature, and to 46.42 % and 5.02 % at 50 °C. These results confirm that iron-activated sodium sulfite effectively suppresses oxygen-rich foulant accumulation and re-exposes membrane pores.

Figs. 4e and f show the FTIR spectra of membranes after different pretreatments. MD with untreated SGPW markedly attenuated the characteristic peaks of pristine PVDF: The CF_2 peak at 1172 cm^{-1} disappeared, while new peaks at 1650 cm^{-1} (C=O/NH_2) and 990 cm^{-1} (Si-O-C) appeared [53], indicating complete surface coverage by proteinaceous and silicon-oxygen foulants, consistent with SEM-EDS results [57]. Sodium sulfite alone provided limited recovery, showing partial reappearance of the 990 cm^{-1} peak at

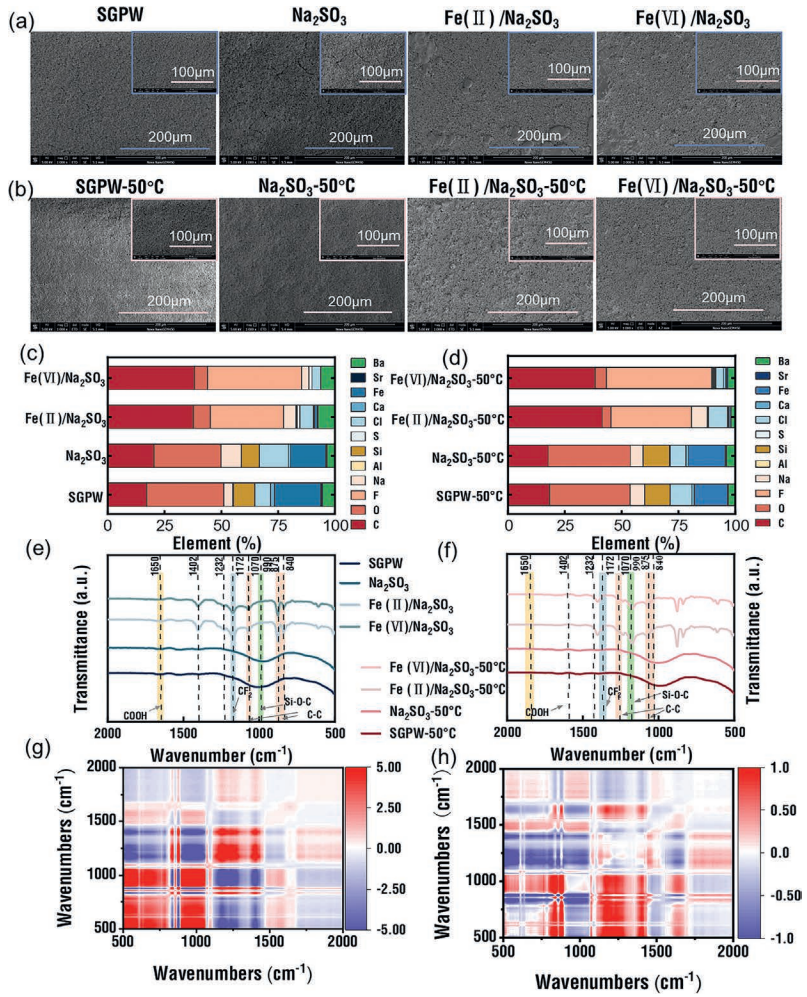


Fig. 4. Effect of Na_2SO_3, Fe(II)/Na_2SO_3 and Fe(VI)/Na_2SO_3 pretreatment on membrane surface properties: (a, b) fouled membrane after MD process, (c, d) EDS analysis, (e, f) FTIR spectra of new membrane and fouled membranes, (g) FTIR synchronous two-dimensional correlation spectroscopy (2D-COS) maps and (h) FTIR asynchronous 2D-COS maps (red indicates positive correlation, blue indicates negative correlation; darker shades indicate stronger correlations). Condition: Fe(II) = 1 mmol/L, Fe(VI) = 1 mmol/L, Na_2SO_3 = 2 mmol/L, SGPW = 200 mL.

room temperature but weaker response under thermal activation, suggesting temperature-sensitive removal of Si-O-C species. In contrast, iron-based activation achieved much greater restoration. At room temperature, both Fe(II)- and Fe(VI)-activation largely recovered the membrane's functional groups, and thermal activation further enhanced this effect: The 1650 and 990 cm^{-1} peaks diminished while the 1172 cm^{-1} CF_2 peak nearly returned to its original intensity. The Fe(VI)-thermal system produced spectra most similar to the pristine membrane, confirming its superior fouling removal efficacy.

Beyond FTIR, synchronous (Fig. 4g) and asynchronous 2D-COS (Fig. 4h) analyses elucidated the correlation and kinetics of organic-inorganic foulant removal under different pretreatments [45]. In the synchronous plot, untreated membranes showed strong auto spectra and positive cross-peaks at 1650 cm^{-1} (C=O/NH_2) and 990 cm^{-1} (Si-O-C), but negligible response at 1172 cm^{-1} (CF_2), indicating complete coverage by organosilicon foulants. Thio-reducing treatment selectively attenuated the 990 cm^{-1} peak while leaving the 1650 cm^{-1} peak unchanged; thermal activation weakened this effect, suggesting temperature-sensitive Si-O-C removal. In contrast, iron activation-especially Fe(VI)-thermal-simultaneously reduced both 1650 and 990 cm^{-1} peaks while restoring the 1172 cm^{-1} CF_2 signal, indicating effective foulant removal and pore re-exposure. Asynchronous analysis confirmed that, in the iron-thermal system, changes at 990 cm^{-1} preceded those at 1650 cm^{-1}, showing that iron activation disrupts the inorganic framework before dispersing organic matter. The thiol-based treatment displayed asynchronous responses only at 990 cm^{-1}, confirming its selective but incomplete action. Overall, Fe(VI)-thermal activation most effectively eliminated organo-inorganic composite fouling by prioritizing inorganic layer dissolution, consistent with FTIR and SEM-EDS results.

These results clearly demonstrate that iron-activated sodium sulfite pretreatment-especially under Fe(VI)-thermal activation-effectively restores membrane surface hydrophobicity and interfacial integrity. This conclusion is strongly supported by complementary findings from SEM-EDS (showing loosening of the fouling layer) and FTIR (revealing functional group recovery), forming a comprehensive and multidimensional validation of the effectiveness of pretreatment.

In the quenching experiments (Fig. 5a), both TBA (1,4-benzoquinone, hydroxyl radical quencher) and MeOH (methanol, sulphate radical quencher) significantly inhibited the removal of UV_{254} by the Fe(II)/Na_2SO_3 and Fe(VI)/Na_2SO_3 systems, with MeOH exhibiting a more pronounced inhibitory effect, indicating that $SO_4^{\bullet-}$ (sulphate radical quencher) is the primary active species responsible for organic degradation in both systems. The Fe(VI)/Na_2SO_3 system exhibited greater sensitivity to quenching agents, suggesting higher radical production. ESR test results (Figs. 5b and c) further confirmed that both systems exhibited typical

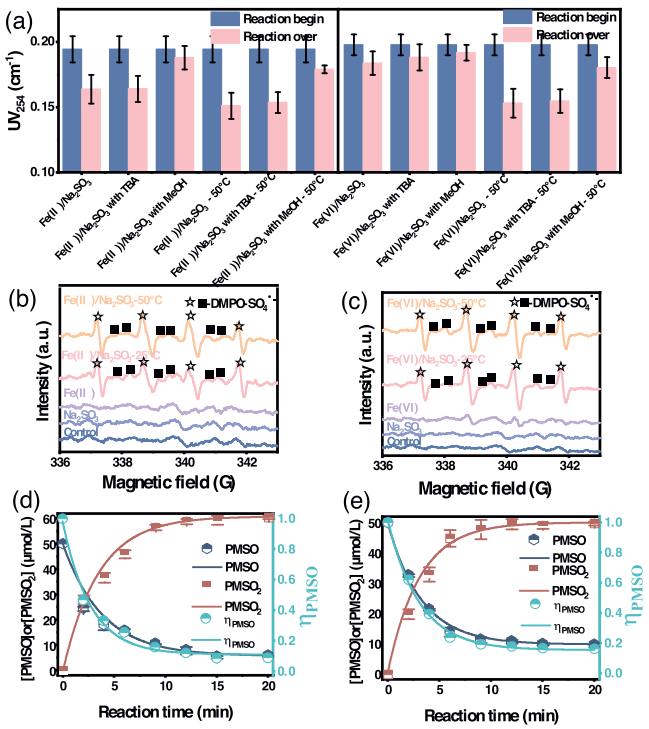


Fig. 5. Mechanism of Fe(II)/Na_2SO_3 and Fe(VI)/Na_2SO_3 oxidation system: (a) Effect of quencher on UV_{254}, (b, c) EPR spectra of DMPO- $SO_4^{\bullet-}$ and (d, e) changes in PMSO and $PMSO_2$ in oxidation system. Condition: Fe(II) = 1 mmol/L, Fe(VI) = 1 mmol/L, Na_2SO_3 = 2 mmol/L, TBA = 10 mmol/L, MeOH = 10 mmol/L, DMPO = 10 μL (scaled down to a 5 ml system), SGPW= 200 mL.

DMPO-$SO_4^{\bullet-}$ signals, with signal intensity significantly enhanced at 50 °C, indicating that increased temperature favors $SO_4^{\bullet-}$ generation. Simultaneously, the signal intensity in the Fe(VI)/Na_2SO_3 system was notably higher than that in the Fe(II)/Na_2SO_3 system. PMSO probe experiments (Figs. 5d and e) showed that the Fe(VI)/Na_2SO_3 system exhibited rapid PMSO conversion and $PMSO_2$ generation at both 25 °C and 50 °C, with conversion rates and yields further enhanced at high temperatures, indicating that temperature not only promotes reactive oxygen species (ROS) generation but also accelerates the formation and reaction of high-valent iron (Fe(IV)/Fe(V)). Mechanistically, the superior removal of hydrophobic organics by Fe(II)/Na_2SO_3 is attributed to efficient $SO_4^{\bullet-}$ generation and the *in-situ* formation of Fe(III), which enhances coagulation and adsorption. In contrast, the Fe(VI)/Na_2SO_3 system exhibits stronger pollutant deposition reduction and liquid entry pressure recovery due to the combined effect of high-valent iron species and $SO_4^{\bullet-}$ radicals, with this synergistic effect being more pronounced at elevated temperatures. In summary, the high oxidation efficiency of the Fe(VI)/Na_2SO_3 system arises from the synergistic effect between $SO_4^{\bullet-}$ and high-valent iron, while Fe(II)/Na_2SO_3 primarily excels in oxidizing hydrophobic organics through efficient radical generation and coagulation-assisted removal.

Fig. S6 (Supporting information) combines Pearson correlation and PLS-PM analyses to clarify the relationships between SGPW characteristics and membrane fouling. Foulant mass correlated strongly and positively with turbidity (0.98), hydrophobic organics (0.97), EEM Regions II (0.94) and IV (0.90) and UV_{254} (0.87), indicating that hydrophobic organics and suspended solids are key foulant contributors. Conversely, it correlated negatively with surface energy (−0.99), contact angle (−0.99), fluorine (−0.98) and LEP (−0.94), implying that fouling decreases membrane hydrophobicity and surface purity. Flux showed positive correlations with zeta potential (0.99), LEP (0.98), contact angle (0.98) and fluorine (0.93), underscoring the roles of colloidal destabilization and hydrophobicity in maintaining performance. Negative correlations with hydrophobic organics (−0.98), turbidity (−0.98), surface energy (−0.95), oxygen (−0.94), UV_{254} (−0.94), ammonia-N (−0.93), conductivity (−0.92) and EEM Regions II-V (−0.94 to −0.90) confirm that organic accumulation and colloidal stability impair flux. The strong inverse relation between Zeta potential and turbidity (−0.99) suggests effective coagulation enhances clarity. Overall, fouling and flux decline are mainly driven by hydrophobic organic buildup and colloidal stability, while reduced colloidal stability mitigates fouling and sustains flux.

To quantitatively reveal the relationships between water quality parameters and MD performance, Fig. 6a and Fig. S7 (Supporting information) present hierarchical clustering and heatmap analyses. These analyses identify intrinsic associations among parameters and their collective impact on membrane fouling [56]. The heatmap displays distinct clustering patterns: Light regions denote strong correlations, while dark regions indicate weak or inverse ones. Multiple independent clusters reflect coordinated variations among physicochemical factors under similar conditions, implying shared sources or interactive effects within the SGPW matrix. The dendrogram (Fig. 6a) further classifies all 24 samples (G1-G24) based on similarities in water quality and fouling behavior. Parameters related to organic loading (TOC, UV_{254}, EEM Regions II and IV) clustered together, highlighting the dominant role of hydrophobic, fluorophore-like organics in driving fouling potential. Another cluster comprising zeta potential, turbidity, and contact angle emphasizes the influence of colloidal stability and surface hydrophobicity. A third cluster, including flux, LEP and foulant mass (FM), reflects the close linkage between membrane performance and chemical-colloidal characteristics. Overall, MD fouling and performance variations are governed by the synergistic effects of organic composition, hydrophobicity, and interfacial electrochemical interactions.

The PLS-PM results (Fig. 6b) identify the key drivers of membrane fouling in SGPW treatment, showing excellent model fit (goodness-of-fit = 0.92). Organic concentration strongly affected hydrophilic/hydrophobic balance (path = 0.97), exerting an indirect influence on fouling (0.88) through compositional changes. Hydrophilic/hydrophobic composition (0.98) and coagulation efficiency (0.80) were the dominant direct determinants. TOC, UV_{254} and EEM Region III (weights = 0.18) emphasized the importance of total organic load and humic/fulvic-like substances. Hydrophobic organics (0.54) contributed slightly more to fouling than hydrophilic ones (0.50), consistent with their higher adhesion and pore-blocking tendency. For the fouling construct, surface parameters-contact angle, foulant mass, LEP and surface energy (weights = 0.15)-were more influential than flux (0.14), indicating that interfacial degradation precedes flux decline. Overall, fouling is governed primarily by hydrophobic organics and coagulation performance, with organic concentration serving as an upstream indirect factor, offering a mechanistic basis for pretreatment optimization.

To elucidate the underlying mechanisms of membrane fouling mitigation, Fig. 6c presents a conceptual model of fouling mitigation by iron-activated sodium sulfite pretreatment. While sodium sulfite alone provides limited oxidative removal, Fe(II)- and Fe(VI)-activation markedly enhance control through combined oxidation, coagulation, and adsorption. In the Fe(II)/sulfite system, Fe(II) generates sulfate radicals ($SO_4^{\bullet-}$) for efficient organic degradation and is oxidized to ferric hydroxide particles that promote coagulation *via* charge neutralization and floc formation. The Fe(VI)/sulfite system forms high-valent Fe(V)/Fe(IV) species and sulfate radicals with even stronger oxidative capacity, collectively degrading complex foulants [58]. Although the roles of Fe(VI) intermediates and

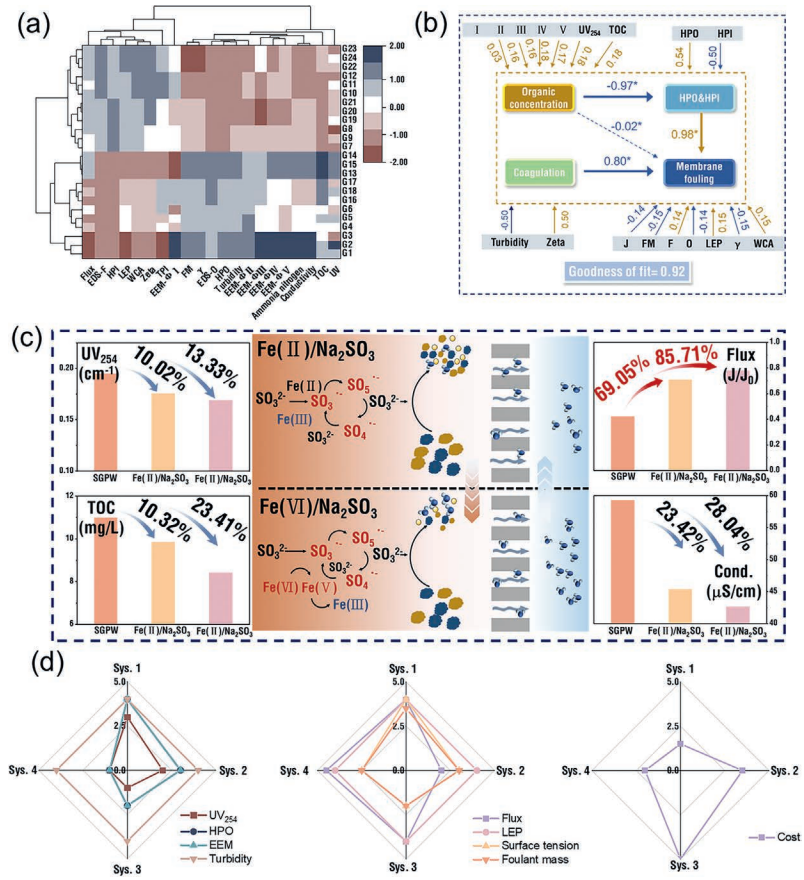


Fig. 6. Correlated factor analysis and mechanism diagram: (a) Cluster heatmap of each characteristic index, (b) PLS-PM modeling to analyze the effect of organic concentration, HPO&HPI and coagulation on the membrane fouling, (c) Fe(II)/Na_2SO_3 and Fe(VI)/Na_2SO_3 oxidation mechanism diagram, (d) Analysis of water purification efficiency, membrane performance stability and economic evaluation in shale gas wastewater treatment using SPC and Na_2SO_3 oxidation. Note: *J*: the normalized flux; FM: foulant mass; O: EDS_O; F: EDS_F; γ: surface tension; Sys. 1: Fe(II)-activated high-concentration sodium percarbonate; Sys. 2: Fe(VI)/Fe(II) mixed-activated low-concentration sodium percarbonate; Sys. 3: Fe(VI)-activated low-concentration sodium sulfite; Sys. 4: Fe(VI)/thermally activated low-concentration sodium sulfite. Nine metrics of four systems, including UV_{254}, HPO, EEM, Turbidity, Flux, LEP, Surface tension, Foulant mass and Cost rated on a scale of 1 to 5 (that is, low to high).

ROS remain debated, their synergistic actions effectively target diverse organics in SGPW.

The interplay between reactive radicals and *in situ* multivalent cations enables efficient removal of membrane-fouling species, significantly improving MD performance. Combined with PLS-PM findings (Fig. 6b), the fouling process can be summarized in three stages: (1) Hydrophobic organics adsorb onto the membrane *via* hydrophobic interactions; (2) this adsorption alters surface energy and reduces hydrophobicity; (3) suspended solids subsequently deposit under convective flow, forming dense foulant layers [14]. Sodium sulfite pretreatment mitigates these processes by (i) degrading hydrophobic organics through oxidation and (ii) enhancing coagulation *via* multivalent cation formation, which lowers turbidity and electrostatic repulsion. These synergistic effects preserve membrane surface properties and effectively suppress fouling.

Overall, membrane fouling mitigation in iron-activated sulfite systems is driven by a synergistic oxidation–coagulation–adsorption mechanism. The combined actions of organic degradation by ROS and particulate removal by Fe(III)-mediated coagulation effectively alter foulant-foulant and membrane-foulant interactions. This comprehensive mitigation strategy significantly improves membrane cleanliness and process stability. Importantly, the results confirm that the hydrophilic/hydrophobic nature of organic matter is the dominant factor influencing membrane fouling behavior, surpassing even the impacts of organic concentration and coagulation effectiveness.

As shown in Fig. 6d, four oxidation systems from previous studies were compared: Fe(II)-activated high-concentration sodium percarbonate (System 1), Fe(VI)/Fe(II) mixed-activated low-concentration sodium percarbonate (System 2), Fe(VI)-activated low-concentration sodium sulfite (System 3), and Fe(VI)/thermally activated low-concentration sodium sulfite (System 4) [14,53]. The evaluation considered three aspects: water quality purification, membrane fouling control, and economic feasibility. System 1 exhibited the highest organic matter removal and excellent membrane performance due to strong hydroxyl radical oxidation and Fe(III)-assisted coagulation, but its high chemical dosage increases operating costs. System 2 achieved a balanced performance, effectively reducing organics and suspended solids at moderate cost *via* Fe(VI)/Fe(II) mixed activation. System 3 showed slightly lower purification and fouling control but offered the lowest pretreatment cost. System 4, by introducing thermal activation to System 3, improved treatment efficiency and membrane performance, and utilizing low-temperature industrial waste heat minimized additional energy costs. In summary, system selection should be scenario-dependent: System 1 is preferred for rapid treatment of high-concentration pollutants, System 2 provides the best overall performance for balanced applications, and System 3 and 4 offer economic advantages, particularly when waste heat is available.

In summary, scheme selection should be based on the target scenario. System 1 is prioritized for rapid reduction of high-concentration organic pollutants. In wastewater treatment projects requiring a balance between treatment effectiveness and operational costs, Systems 2, 3 and 4 are more applicable, with System 2 offering the best overall performance and System 4 demonstrat-

ing outstanding economic viability in scenarios where waste heat is available.

This study systematically investigated the effects of the Fe(II)/Fe(VI)-activated sodium bisulfite pretreatment process on water purification efficiency, membrane surface morphology, and membrane surface performance, and drew the following main conclusions:

(1) Iron-activated sulfite systems markedly enhanced SGPW purification at both room and elevated temperatures. At room temperature, Fe(II)/Fe(VI) systems achieved UV_{254}, TOC and NH_3-N removals of 13.33 %/10.00 %, 12.64 %/10.32 % and 22.68 %/26.60 %, respectively, with hydrophobic fractions reduced to 40.8 % and fluorescence intensity by 11 %. Heating to 50 °C further improved all removals, confirming thermal promotion of pollutant degradation.
(2) Sodium sulfite pretreatment significantly improved MD performance. At room temperature, Fe(II)/Fe(VI) systems raised normalized flux to 69.05 %/80.95 % and reduced conductivity by 24.93 %/28.74 %. At 50 °C, flux further increased to 80.95 %/85.70 % with comparable conductivity reductions, demonstrating enhanced synergistic effects under thermal activation.
(3) Pretreatment restored membrane properties *via* oxidation–coagulation–adsorption synergy. Fe(II)/Fe(VI) systems raised LEP recovery to 86.70 %/88.37 % and reduced foulant mass by 40.42 %/47.57 % at room temperature, improving to 89.20 %/90.86 % and 44.32 %/61.79 % at 50 °C. SEM-EDS, FTIR and surface analyses confirmed reduced fouling and preserved hydrophobicity.
(4) Fouling control was governed by synergistic oxidation–coagulation–adsorption. Organic concentration, hydrophobicity, and coagulation efficiency were the key determinants: organic concentration indirectly modulated hydrophobic balance, while hydrophobicity and coagulation directly controlled fouling intensity.

In summary, the iron-based activated sodium sulfite pretreatment process significantly improves water purification efficiency, enhances membrane properties, and alleviates membrane fouling through multiple synergistic effects, providing important technical support for the efficient treatment of SGPW.

CRediT authorship contribution statement

Yuan Huang: Writing – original draft, Visualization, Validation, Formal analysis, Data curation. **Suhua Gu:** Writing – original draft, Formal analysis, Data curation. **Haiqing Chang:** Writing – review & editing, Supervision, Project administration, Methodology, Funding acquisition, Formal analysis, Conceptualization. **Bo Lai:** Writing – review & editing, Supervision, Project administration.

Declaration of competing interest

The authors declare that they have no known competing financial interests or personal relationships that could have appeared to influence the work reported in this paper.

Acknowledgments

The work was jointly supported by the National Natural Science Foundation of China (Nos. 52570009, 52370082) and Sichuan Science and Technology Program (No. 2023YFH0053).

Supplementary materials

Supplementary material associated with this article can be found, in the online version, at doi:10.1016/j.cclet.2026.112476.

References

[1] Y. Gan, H.M. El-Houjeiri, A. Badahdah, et al., Nat. Commun. 11 (2020) 824.
[2] C.L. Weber, C. Clavin, Environ. Sci. Technol. 46 (2012) 5688–5695.
[3] E.I. Nduagu, I.D. Gates, Environ. Sci. Technol. 49 (2015) 8824–8832.
[4] C. Sun, H. Nie, W. Dang, et al., Energ. Fuel 35 (2021) 6359–6379.
[5] R.D. Vidic, S.L. Brantley, J.M. Vandenbossche, D. Yoxtheimer, J.D. Abad, Science 340 (2013) 1235009.
[6] H.J. Khan, E. Spielman-Sun, A.D. Jew, et al., Environ. Sci. Technol. 55 (2021) 1377–1394.
[7] D.L. Shaffer, L.H.A. Chavez, M. Ben-Sasson, et al., Environ. Sci. Technol. 47 (2013) 9569–9583.
[8] H. Chang, T. Li, B. Liu, R.D. Vidic, M. Elimelech, J.C. Crittenden, Desalination 455 (2019) 34–57.
[9] H. Chang, N. Liu, F. Qu, et al., Chem. Eng. J. 474 (2023) 145576.
[10] H. Chang, T. Li, B. Liu, et al., Crittenden, Environ. Int. 130 (2019) 104869.
[11] K.M. Shah, I.H. Billinge, X. Chen, et al., Desalination 538 (2022) 115827.
[12] Y. Liu, P. Tang, Y. Zhu, et al., Chem. Eng. J. 416 (2021) 129100.
[13] M.M. Zico, B.C. Ricci, B.G. Reis, N.C. Magalhaes, M.C.S. Amaral, Sep. Purif. Technol. 264 (2021) 118356.
[14] S. Gu, F. Qu, D. Qu, et al., Water Res. 262 (2024) 122139.
[15] V. Vatanpour, R. Ardic, B. Esenli, et al., Sep. Purif. Technol. 345 (2024) 127336.
[16] X. Cheng, J. Lian, Z. Ren, et al., Water Res. 204 (2021) 117622.
[17] H. Cho, Y. Choi, S. Lee, Desalination 437 (2018) 195–209.
[18] E. Gontarek-Castro, R. Castro-Muñoz, Green Chem. 26 (2024) 164–185.
[19] Y. Zou, Y. Hu, D. Tian, et al., Chin. Chem. Lett. 35 (2024) 109090.
[20] M. Lu, H. Chang, Z. Yan, et al., Sep. Purif. Technol. 341 (2024) 126927.
[21] A. Abdel-Karim, S. Leaper, C. Skuse, et al., Chem. Eng. J. 422 (2021) 129696.
[22] H. Chang, Z. Ma, D. Qu, et al., Water Res. 266 (2024) 122434.
[23] W. Zhang, W.C. Fu, Z.H. Wang, et al., Sep. Purif. Technol. 377 (2025) 134226.
[24] L. Jiang, L. Chen, L. Zhu, Desalination 485 (2020) 114457.
[25] A. Alkhatib, M. Ayari, A. Hawari, Chem. Eng. Process. 167 (2021) 108517.
[26] X. Wei, B. Zhao, X. Li, et al., J Membr. Sci. 407 (2012) 164–175.
[27] G. Kang, Y. Cao, J Membr. Sci. 463 (2014) 145–165.
[28] J. Zhao, S. Wang, S. Zhao, et al., Chin. Chem. Lett. 36 (2025) 109883.
[29] Z. Ji, J. Wang, Z. Yan, et al., Sep. Purif. Technol. 351 (2024) 128124.
[30] B. Qiu, J. Liu, Y. Liu, et al., J. Environ. Manage. 347 (2023) 119094.
[31] E. Gontarek-Castro, R. Castro-Muñoz, M. Lieder, Crit. Rev. Env. Sci. Tec. 52 (2022) 2104–2149.
[32] V. Vatanpour, A. Yuksekdag, M. Agtas, et al., Carbohyd. Polym. 299 (2023) 120230.
[33] J. Li, J. Wu, H. Sun, F. Cheng, Y. Liu, Desalination 380 (2016) 43–51.
[34] Z. Lu, Z. Yan, H. Chang, et al., Chem. Eng. J. 492 (2024) 151981.
[35] Y. Huang, H. Chang, X. Cheng, H. Liang, Sep. Purif. Technol. 360 (2025) 130619.
[36] S. Waclawek, H.V. Lutze, K. Grübel, et al., Chem. Eng. J. 330 (2017) 44–62.
[37] W. Li, Y. Lou, A. Fang, K. Feng, D. Xing, Chem. Eng. J. 394 (2020) 124920.
[38] Q. Xiao, S. Yu, Chem. Eng. J. 417 (2021) 129115.
[39] K. Tian, L. Hu, L. Li, et al., Chin. Chem. Lett. 33 (2022) 4461–4477.
[40] J. Zhao, Q. Song, Q. He, J. Environ. Chem. Eng. 11 (2023) 110383.
[41] K. Chen, G. Zhu, X. Huang, et al., Sep. Purif. Technol. 328 (2024) 125112.
[42] W. Liu, B. Liu, X. Li, Chemosphere 308 (2022) 136302.
[43] J. Cao, W. Nie, L. Huang, et al., Appl. Catal. B: Environ. 241 (2019) 18–27.
[44] X. Cheng, D. Sai, X. Luo, et al., Water Res. 261 (2024) 122013.
[45] B. Yang, L. Tian, P. Zhou, et al., Nat. Commun. 16 (2025) 5998.
[46] X. Chen, Z. Huang, Z. Ji, et al., Environ. Technol. Inno. 19 (2020) 100897.
[47] N. Li, S. Wu, H. Dai, et al., Chem. Eng. J. 450 (2022) 137976.
[48] S. Pang, J. Jiang, J. Ma, et al., Environ. Sci. Technol. 45 (2011) 307–312.
[49] Y. Ye, N. Yang, L. Xiao, et al., Environ. Sci. Pollut. R. 30 (2023) 30122–30129.
[50] F. Xiao, X. Zhang, J. Ma, Sep. Purif. Technol. 68 (2009) 273–278.
[51] J. Wang, Y. Liu, L. Feng, Y. Wang, H. Jia, J. Water Process Eng. 49 (2022) 103183.
[52] L. Guo, M. Lu, Q. Li, et al., Bioresource Technol. 171 (2014) 22–28.
[53] H. Chang, Y. Huang, S. Gu, X. Cheng, F. Qu, Water Res. 288 (2025) 124533.
[54] P. Tang, W. Xie, A. Tiraferri, et al., Water Res. 196 (2021) 120920.
[55] Z. Yan, Z. Lu, X. Chen, et al., Sep. Purif. Technol. 289 (2022) 120787.
[56] Y. Zhu, F. Qu, D. Qu, et al., J Membr. Sci. 713 (2025) 123259.
[57] P. Pisciella, M. Pelino, J. Eur. Ceram. Soc. 25 (2005) 1855–1861.
[58] B. Yang, G. Ying, L. Zhang, et al., Water Res. 45 (2011) 2261–2269.